·Article · Advances in Polar Science
doi: 10.12429/j.advps.2022.0050 June 2023 Vol. 34 No. 2: 125-143

Investigating the impact of atmospheric parameters on sea ice variability in and around Svalbard

Dency V PANICKER[1], Bhasha VACHHARAJANI[2*] & Rohit SRIVASTAVA[3]

[1] Department of Physics, School of Energy Technology, Pandit Deendayal Energy University, Gandhinagar, Gujarat, India;
[2] Department of Mathematics, School of Technology, Pandit Deendayal Energy University, Gandhinagar, Gujarat, India;
[3] Department of Physics, School of Energy Technology, Pandit Deendayal Energy University, Gandhinagar, Gujarat, India

Received 30 May 2022; accepted 4 April 2023; published online 30 June 2023

Abstract Recent research has shown that winter warmings are phenomenally high compared to summer warmings over the poles, especially over the Arctic. Taking the current scenario into account, this paper attempts to understand the atmospheric variables causing sea ice variability over and around the region of Svalbard for seasons; winter, spring, summer and autumn for the span of 42 years (1979–2021). The variability in atmospheric and oceanic parameters namely temperature, precipitation, wind speed, and sea surface salinity are analysed over inter-spatial, inter-seasonal and inter-annual domains. Winters are characterized by inter-annual increasing trend in temperature. During 1981–1990 the rise from the decadal mean is found to be 0.39 K·a^{-1}, during 1991–2000 it is 0.20 K·a^{-1}, during 2001–2010 it is 0.04 K·a^{-1} and during 2011–2020 it is 0.23 K·a^{-1}. Interestingly while considering inter-spatial domains, the region southwest to Svalbard seems to be wetter (0.05 mm·(10 a)$^{-1}$) compared to its northeast (–0.03 mm·(10 a)$^{-1}$). Across all the three domains, wind speeds are highest during autumn and then decrease subsequently through summer, spring and are least during winter. Wind is predominantly from the south, and hence it is suspected to carry hot Atlantic air. Additionally, the significant role of salinity in the ocean also plays a key role in governing the fate of sea ice conditions. The long-term forecasts of temperature over sea ice of Svalbard are alarming especially for the winter ice (r=–0.84). Correlation matrices between atmospheric and sea ice parameters are shown to gain a better understanding on their inter relation.

Keywords **Svalbard, northeast Svalbard, southwest Svalbard, temperature, precipitation, wind speed, sea ice concentration**

Citation: Panicker D V, Vachharajani B, Srivastava R. Investigating the impact of atmospheric parameters on sea ice variability in and around Svalbard. Adv Polar Sci, 2023, 34(2): 125-143, doi: 10.12429/j.advps.2022.0050

1 Introduction

During the latest decades, Arctic temperatures have increased to 3.1 °C at an intensified rate compared to the global mean (1.02 °C) (IPCC, 2021), which has been attributed to the disappearance of sea ice cover, area, and extent, resulting in ice-atmosphere feedbacks (Bintanja and van der Linden, 2013). Furthermore, precipitation in the Arctic has increased by 30%–60% during this decade in response to atmospheric moistening (Zhang et al., 2013). An increase in both temperature and precipitation over the Arctic is projected to accelerate the decline in sea ice during the twenty-first century (Bintanja and Selten, 2014). It is already known that the Arctic plays a crucial role in governing the earth's climate as a whole. A small change in the area of sea ice over this region can alter the planet's climatic order, leading to an increase in temperature (Overland et al., 2019). Because less ice means less albedo, only a small amount of incoming solar radiation is scattered

*Corresponding author, E-mail: bhasha.vachharajani@sot.pdpu.ac.in

back into the atmosphere. The third Intergovernmental Panel on Climate Change report had already pointed towards the sensitivity of the climate in the Svalbard region (Zillman, 2001). Historical climate observations on Svalbard are well documented (Førland et al., 1997), but are largely focused on the west of Svalbard (Ivanov, 2019). However, a recent report by the Norwegian Environmental Agency has called attention to the less explored regions of Spitsbergen (Hanssen-Bauer et al., 2019).

Svalbard is one of the key regions for air-sea ice interactions and transport processes in the passage between Greenland and Fram Strait, which are located in the high latitudes of the North Atlantic. Additionally, sea ice conditions around Svalbard, in particular sea ice concentration (SIC), sea ice area (SIA), and sea ice extent (SIE), are influenced by (1) the geographical setting, such as the seabed topography of Svalbard, (2) regional conditions, and (3) the patterns and properties of the regional ocean currents (Walczowski et al., 2017). Svalbard is situated adjacent to both the Arctic and Atlantic water masses. The sea ice over this region is influenced by warm, saline water from the Atlantic to the Arctic Ocean along the west of Svalbard, whereas cold, less saline water from the Arctic to the Atlantic impacts the east of Svalbard (Svendsen et al., 2002). The latter current continues around South Cape and prevails as a coastal current along West Spitsbergen's shelf. Thus, Atlantic water mixes with Arctic water on the shelf and is advected into the open fjords as transformed Atlantic water (Nilsen et al., 2016).

In regions surrounded by coastlines, ice deformation is often seen to be strong when winds are directed onshore. These processes may form much thicker sea ice by dynamic thickening than that could have been formed by thermodynamic growth (Haas et al., 2009). For Storfjorden, external sea ice from the Barents Sea may be advected into the central fjord by the southerly winds, which can lead to significant dynamic ice growth. Little information is available about these events and the resulting concentrations and thicknesses due to lack of data (Gerland and Hall, 2006), which is mostly because of safety and logistical constraints.

The key goal of this study is to quantify the role of the atmospheric and oceanic variables (temperature, precipitation, wind speed, and sea surface salinity) in sea ice melting over the regions around Svalbard utilizing remote sensing data at inter-seasonal, inter-spatial, and inter-annual domains. Here satellite data of SIC is used to establish the role of local melting in explaining the near absence of sea ice around the northeast (NE) part of Svalbard, Svalbard, and the southwest (SW) part of Svalbard. Estimated annual melting rates are then correlated with atmospheric observations to identify the contribution of these parameters in determining the state and fate of sea ice. The precise magnitude by which these atmospheric parameters can impede the growth or decay of sea ice over Svalbard remains unknown. However, because Svalbard is an archipelago with a small population, such studies highlight the importance of better understanding the region for adaptation and mitigation planning.

2 Datasets and methodology

For the purpose of this paper, the region around Svalbard is considered due to its intertwined topography, which is shared by the Atlantic and the Arctic waters. The source of the datasets and the methodology adopted are elaborately explained in the subsequent sections (2.1 and 2.2).

2.1 Datasets

This paper consists of three variants of datasets: (1) atmospheric variables, (2) oceanic variables, and (3) cryospheric variables. All the datasets are accessed remotely to investigate the impact of atmospheric parameters on sea ice conditions for the period 1979–2021 (a span of 42 years). The atmospheric variables used are: air temperature (K), precipitation (m), and wind speed ($m \cdot s^{-1}$), and the oceanic variable used is sea surface salinity (PSU). To estimate the sea ice condition prevailing over the region, SIC is used. These datasets are evaluated exclusively on the basis of their availability in spatial and temporal domains. All the details regarding its spatiotemporal coverage and spatiotemporal resolutions are mentioned in Table 1.

Table 1 Temporal and spatial coverage of remote sensing SIC, temperature, precipitation and wind (speed and direction) data that are used in this study

	SIC	10-m temperature	Total precipitation	10-m wind	Sea surface salinity
Temporal coverage	1979–present	1979–present	1979–present	1979–present	1979–present
Spatial coverage	Pan-Arctic Ocean	Global	Global	Global	Global
Spatial resolution	25 km×25 km	25 km×25 km	25 km×25 km	25 km×25 km	25 km×25 km
Temporal resolution	monthly	monthly	monthly	monthly	monthly
Source	NSIDC	ERA-5 ECMWF reanalysis	ERA-5 ECMWF reanalysis	ERA-5 ECMWF reanalysis	Climate and Forecast (CF) Metadata Convention v1.6

2.1.1 Atmospheric data

To study the meteorological shift over and around Svalbard, atmospheric variables comprising air temperature at 2 m (K), total precipitation (m), 10-m wind speed ($m \cdot s^{-1}$), and 10-m wind direction are considered. All of the datasets are derived from the ERA-5 ECMWF reanalysis with a spatial resolution of 25 km×25 km and a one-month time interval. The term "air temperature above 2 m" refers to the air's temperature at a height of 2 m over land, water, or inland waters. By interpolating between the lowest model level and the earth's surface while taking the atmospheric conditions into consideration, the temperature at 2 m is estimated. This parameter is measured in degrees Kelvin (K). By deducting 273.15, the temperature recorded in degrees Kelvin can be converted to degrees Celsius (°C). Another parameter, total precipitation, yields the accumulated liquid and frozen water, comprising rain and snow that falls to the earth's surface. This parameter gives the sum of large-scale precipitation and convective precipitation. It does not include fog, dew, or the precipitation that evaporates in the atmosphere before it lands on the surface of the earth. The unit of this parameter is depth in metres of water equivalent. The parameter wind speed gives the horizontal speed of the wind, or movement of the air, at a height of 10 m above the surface of the earth. The unit of wind speed is $m \cdot s^{-1}$.

2.1.2 Oceanic data

The salinity is a parameter that connects the oceanic sand and cryospheric elements. Therefore, the salinity data is acquired from CMIP6 (Coupled Model Intercomparison Project Phase 6) climate projections. This parameter addresses the salt concentration close to the ocean's surface. The variable is measured in practical salinity units (PSU).

2.1.3 Cryospheric data

SIC is one of the remote sensing products that has been available since 1979. The parameter is defined as the fraction of a pixel or grid cell in a satellite image or other gridded product that is covered with sea ice. SIC products have been validated and widely used (Onarheim et al., 2018), in similar studies. The SIC product is provided by NSIDC (National Snow and Ice Data Center) (Table 1), which is derived from Special Sensor Microwave Imager (SSM/I) and Special Sensor Microwave Imager Sounder (SSMI/S) (https://nsidc.org/ data/G02135/versions/3, accessed on 24 May, 2022). The SIC is estimated to understand the precision of the NASA Team algorithm (Cavalieri et al., 1996). The accuracy of each SIC pixel is ±15% in the summer and ±5% in the winter.

3 Methodology

From Table 1, it is evident that the spatial and temporal resolution of SIC is the same as that of the atmospheric and oceanic variables (temperature, precipitation, wind speed, and sea surface salinity), which made the analyses and study much simpler. The recent declining trend in sea ice over and around Svalbard has drawn special attention to the region; therefore, the focus of the paper is heavily centred on the NE and SW parts of Svalbard as well as the entire region. The considered regions are depicted in Figure 1. The NE part of Svalbard lies between 30°E–50°E and 81°N–84°N and the region around Svalbard falls under the coordinates 10°E–30°E and 76°N–81°N. Finally, the SW part of Svalbard lies between 170°W–10°E and 71°N–76°N. Time series of all parameters are obtained by averaging over each domain separately during different seasons. The four seasons considered are winter (DJF), spring (MAM), summer (JJA), and autumn (SON) for the span of 42 years (1979–2021). Further, linear regression is applied to evaluate the SIC and temperature trends, and the *t*-test is used to estimate the statistical significance level. The regression analysis gives slope and intercept values, which are shown in Figure 2. The monthly temperature anomaly ($K \cdot a^{-1}$) is estimated by calculating the difference between the monthly average from 1979 to 2021 and the value for the corresponding month using the formula (1).

$$\Delta = x - \mu \tag{1}$$

where, Δ represents the anomaly or deviation of the observed value (x) from the mean value (μ).

To estimate the winter warming over the three considered region, years 1979–2021 is divided into six years each, and its average temperature is estimated for the months December, January and February (DJF). The calculation of temperature rise ($K \cdot a^{-1}$) is made using the formulas (2) and (3).

$$\Delta T_{\uparrow} = \frac{\Delta T_{\text{abs}}}{\Delta T_{\text{prev}}} \tag{2}$$

where $\Delta T_{\uparrow}$ shows the temperature change, mostly temperature rise, ΔT_{abs} represents the absolute change in temperature and ΔT_{prev} shows the previous change in temperature.

$$\Delta T_{\text{abs}} = V_{\text{n}} - V_{\text{p}} \tag{3}$$

where ΔT_{abs} shows the absolute change in temperature (as mentioned previously), V_{n} represents the new value and V_{p} shows the previous value.

Further precipitation data is also segregated based on different seasons over the span of 42 years. Additionally, the wind speed and wind direction over the considered domains are represented using wind rose diagram for each season. The legends represent the speed of the wind over the region, and the curvature shows the direction in which they blow. To analyse the oceanic influence on the sea ice condition over the considered region, sea surface salinity (SSS) is considered. Monthly average data is accumulated over the span of 42 years, and hovmoller plot is created to understand

the seasonal variation of the parameter in a temporal framework. Further, the correlation analyses and linear regression analyses are performed by the seasonal monthly mean of cryospheric and atmospheric variables. The correlation matrix is used to understand the linkages and directions, whereas the regression analyses is used to understand the strength between SIC and atmospheric and oceanic factors (temperature, precipitation, wind speed, and SSS). The temporal profiles for all the parameters based on all three considered regions are finally plotted to understand their dependence on sea ice conditions during the winter.

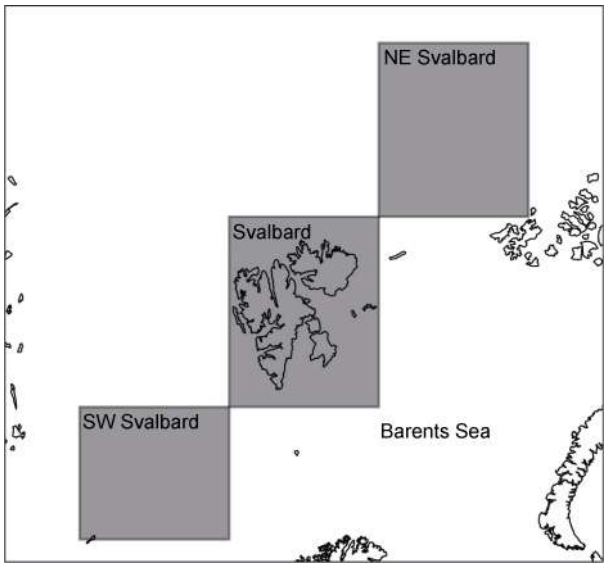

Figure 1 Region of interest: northeast part of Svalbard, Svalbard, and southwest part of Svalbard.

4 Results and discussions

4.1 Variability in air temperature

Through 1979–2021, time series of average temperature over three domains (the NE part of Svalbard, Svalbard, and SW part of Svalbard) during winter (DJF), spring (MAM), summer (JJA), and autumn (SON) months show a clear heterogeneity in observed seasonal temperature trends (Figure 2). The equation of the trend line along with the values of the slopes, intercept, r^2, and p-value are represented in Figure 2. The air temperature over NE part of Svalbard (Figure 2a) varies from 244–276 K. The summer air temperature shows a gradual incline during the entire span of 42 years. However, the seasons of winter and spring are seen to show fluctuation, except that the range of the parameter is significantly lower compared to autumn and summer. From the slope values, it is evident that the winter slope is 0.20, which is greater than any other season. Temperature rise rates are 0.38, –0.56, 0.58, 1.23, 0.62, and 0.20 K·a^{-1} from 1985 to 1990, 1991 to 1996, 1997 to 2002, 2003 to 2008, 2009 to 2014, and 2015 to 2020. From the rates, it is evident that the regions experience stronger winter warming than summer warming. This phenomenon is also prevalent over the Arctic, namely Arctic Winter Warming (AWW), which is one of the key features of Arctic Amplification. Such processes have been attributed to the retreat of sea ice and the resulting ice atmosphere feedback (Holland and Stroeve, 2011). The most notable feature of the area is that the region, being closer to the north, experiences a lower range of air temperature compared to the other two regions of study.

Over Svalbard (Figure 2b), the range of temperatures is higher than that of the NE part of Svalbard, and the range lies between 248 and 280 K. Here, the range during summer and autumn is almost the same. However, the slope value of autumn is seen to be slightly higher (0.06) compared to that of summer (0.02). Similar to the NE part, Svalbard also experiences a high degree of transition during winter with a slope value of 0.24. The spring and winter seasons experience similar fluctuations in values as those over the previous considered area of interest. Here the rates are, 0.21, 0.10, 0.49, 1.13, 0.59, and 0.21 K·a^{-1} from 1985 to 1990, 1991 to 1996, 1997 to 2002, 2003 to 2008, 2009 to 2014, and 2015 to 2020 respectively. Furthermore, an interdecadal comparison of temperature rises during winters revealed that the rise was 0.39 K·a^{-1} during 1981–1990, 0.20 K·a^{-1} during 1991–2000, 0.04 K·a^{-1} during 2001–2010, and 0.23 K·a^{-1} during 2011–2020. Additionally, around 2015, the winter temperature trendline intersected with the spring temperature trendline, indicating that the land experienced higher temperatures in the spring than in the summer during the recent period. Lastly, in the SW part of Svalbard (Figure 2c), the range of air temperatures lies between 262 and 280 K. Over the region, the value of the lower limit is slightly higher compared to that over Svalbard. Here also, the slope during winter season is higher compared to all other seasons, with a value of 0.10.

The most notable feature of this region is that the fluctuation of temperature during spring remains unchanged. Temperature rates in the SW part of Svalbard are, –0.23, 0.49, –0.21, 0.61, 0.18, and 0.04 K·a^{-1} from 1985 to 1990, 1991 to 1996, 1997 to 2002, 2003 to 2008, 2009 to 2014, and 2015 to 2020 respectively. When bifurcating the temporal scale to 1980–2000 and 2000–2020, it is found that the rise in temperature during latter years (2000–2020) are high compared to that during the former span (1980–2000). From the trend line it is obvious that the slope is high during winter, summer and autumn. However, during spring the pattern remains almost constant with range close to ~272 K.

Overall, Figure 2 shows that winter warmings are stronger than summer warmings, which further reduces the magnitude of the annual temperature cycle. Additionally, it is also known that more pronounced warming of cold precipitation than warm spells lead to a reduction of short-term (intra-seasonal) temperature variability. Such heating of cold spells is responsible for the decrease in inter-annual variability in seasonal temperatures, since

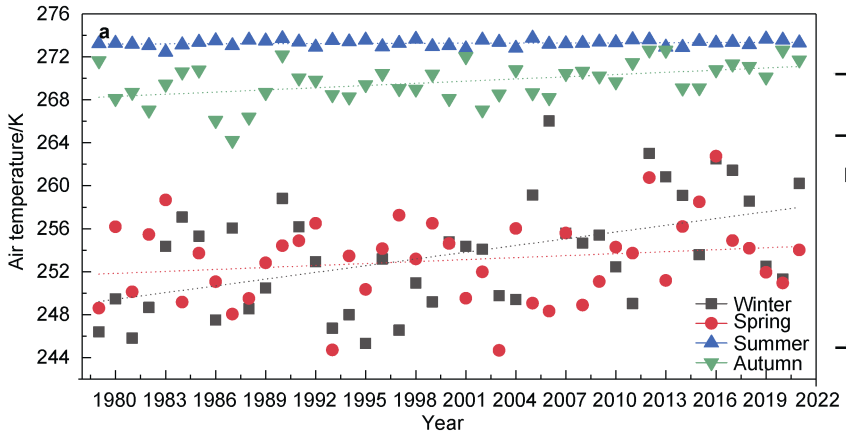

Season	Winter	Spring	Summer	Autumn
Intercept	−164.57 ± 112.19	130.34 ± 94.34	265.83 ± 7.10	133.44 ± 41.15
Slope	0.20 ± 0.00	0.06 ± 0.04	0.00± 0.00	0.06 ± 0.02
r^2	0.23	0.01	0	0.19
p-value	$p < 0.1$	$p > 0.1$	$p > 0.1$	$p < 0.1$

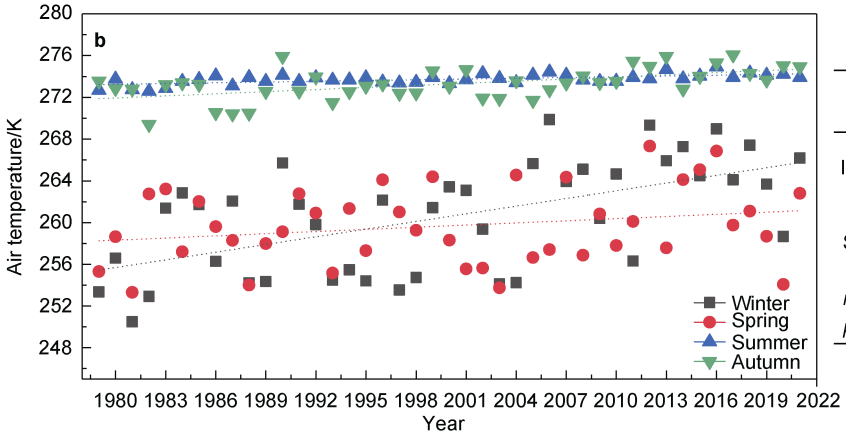

Season	Winter	Spring	Summer	Autumn
Intercept	−229.80 ± 106.45	122.19 ± 88.66	224.97 ± 9.50	138.43 ± 31.57
Slope	0.24 ± 0.05	0.06 ± 0.04	0.02 ± 0.00	0.06 ± 0.01
r^2	0.32	0.03	0.37	0.29
p-value	$p < 0.1$	$p > 0.1$	$p > 0.1$	$p < 0.1$

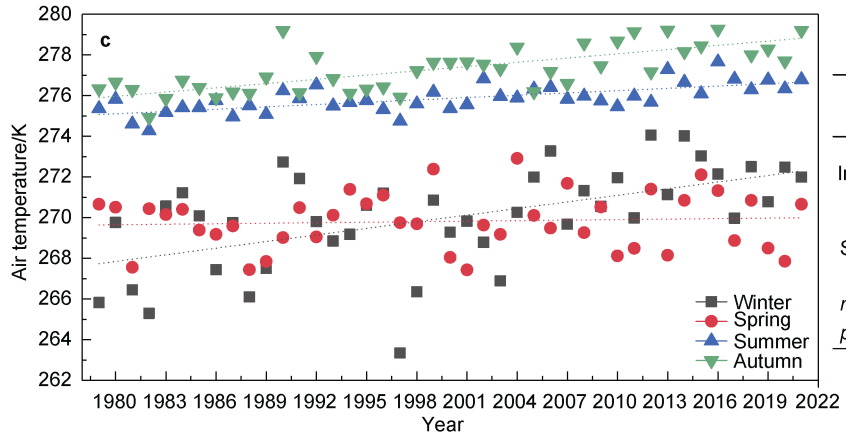

Season	Winter	Spring	Summer	Autumn
Intercept	53.40± 50.72	253.12 ± 34.36	200.11 ± 12.59	138.15 ± 20.89
Slope	0.10 ± 0.02	0.00 ± 0.00	0.03 ± 0.00	0.06 ± 0.01
r^2	0.29	−0.01	0.45	0.5
p-value	$p < 0.1$	$p > 0.1$	$p < 0.1$	$p < 0.1$

Figure 2 Seasonal air temperature during winter, spring, summer and autumn over southwest part of Svalbard (**a**), northeast part of Svalbard (**b**) and Svalbard (**c**) for the span 1979–2021. Linear regression analysis with intercept, slope, r^2 and *p*-value of air temperature during winter, spring, summer and autumn over, northeast part of Svalbard, Svalbard, and southwest part of Svalbard.

relatively warm seasons will experience a weaker warming trend than relatively cold seasons. Finally, seasonal precipitation trends cause the magnitude of individual precipitation (snow) events to increase while the frequency of precipitation events remains unchanged in the projected climate, which will be discussed in subsequent sections. Apart from time series analyses, the anomalies considered in Figure 3 show an overall increase in air temperature up to 2021 (from 2000), which further helps understand the air temperature prevailing over the considered region. During the winter (Figure 3a), the range of anomalies lies between –8 and 10 K, which is the highest compared to any other season. The slope is seen to be almost the same and lower for Svalbard and the SW part of Svalbard compared to the NE part of Svalbard. Further during spring (Figure 3b), the range is seen to lie between –6 and 6 K. The slope of the temperature anomaly is observed to be greater for Svalbard, followed by the SW, and finally the NE parts of Svalbard.

During summer (Figure 3c), the variation in anomaly is higher over the SW part of Svalbard compared to the other two domains. However, the trend in autumn (Figure 3d) is seen to be an exact match with that in spring, with some variation in the range. The latter 20-year period (1980–2000) is characterised by a general decrease (although relatively weak) in the temperature of surrounding waters (Figure 3). Therefore, for all the seasons, the years 2000–2020 are seen to have higher trends (positive) than the years 1980–2000. Here it is found that the temperature anomalies have maximum variations during winter (–8 to 10 K), and then the range goes down with spring (–6 to 6 K), summer (–1.5 to 1.5 K), and autumn (–8 to 6 K).

The dynamics of warming over Svalbard prior to the 1930s are still not fully understood, while the warming from the 1960s to the mid-1990s is clearly linked to atmospheric feedback and circulation patterns favouring increased southerly and southerly winds in the Svalbard area (Hanssen-Bauer and Førland, 1998). This agrees well with the findings of the researchers in the past (Rigor et al., 2000) which stated that more than half the warming over the eastern Arctic Ocean and the cooling over the Labrador Sea from the 1970–1990 is accounted for by the Arctic Oscillation (AO). Not only that, the Northern Annual Mode (NAM) is partly responsible for the Arctic warming in this period (Polyakov et al., 2003). The recent decade, on the other hand, shows rather different patterns. The warmest winters in Svalbard occurred after 2000, several of these winters were characterised by average or low AO. Lately, it has also been understood that the recent loss of Arctic sea ice is responsible for the high Arctic temperatures. This loss is not only directly contributing to the heat budget of the atmosphere in the area but also leading to a modification of large-scale atmospheric circulation towards the Warm Arctic Cold Continents (WACC) wind pattern (Overland et al., 2014).

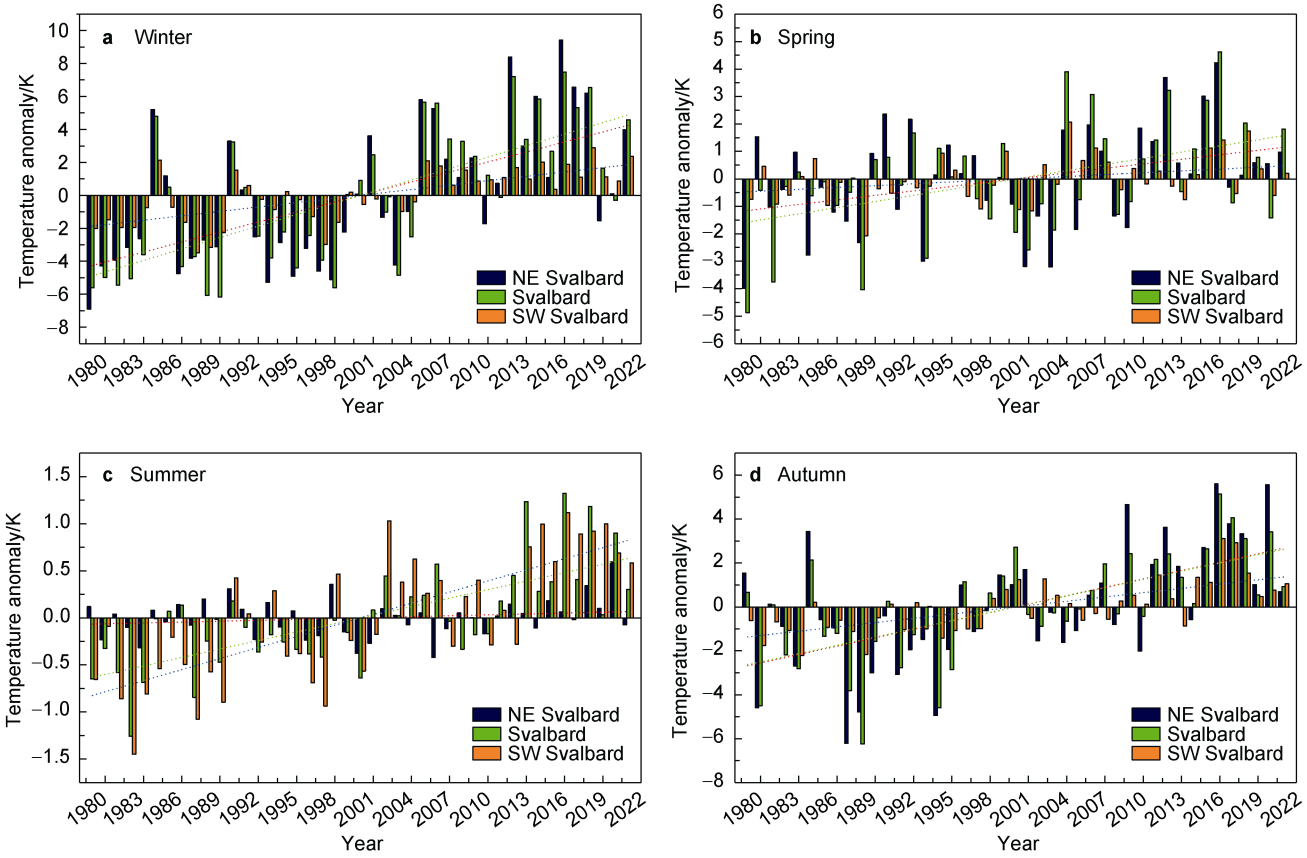

Figure 3 Air temperature (K) anomaly over northeast part of Svalbard, Svalbard and southwest part of Svalbard for winter (**a**), spring (**b**), summer (**c**), and autumn (**d**) for the span 1979–2021.

4.2 Variability in precipitation

From the above discussions on the temperature patterns over Svalbard, the location of the island is well understood. Svalbard is located at the main gateway for both atmospheric and oceanic heat transport. The final destination of such transports is always the Central Arctic. In the further tropics, cyclone activity is the main atmospheric mechanism of poleward heat transport, transporting warm and moist air masses together with high winds and precipitation (Trenberth and Stepaniak, 2003). For a better understanding of the region, the seasonal variation of precipitation over the SW part of Svalbard, the NE part of Svalbard, and Svalbard itself is represented in

Figure 4. The spatial distribution of precipitation is primarily governed by local topography, as is the case with temperature, and secondarily by a negative lateral gradient from southwest to northeast Svalbard winds, which will be discussed in the next section.

Over the NE part of Svalbard (Figure 4a) the range of precipitation is found to lie between 0 to 1.80×10^{-3} m, which is significantly low compared to Svalbard and the SW part of Svalbard. During autumn, the NE region of the country receives the most precipitation, with an average of

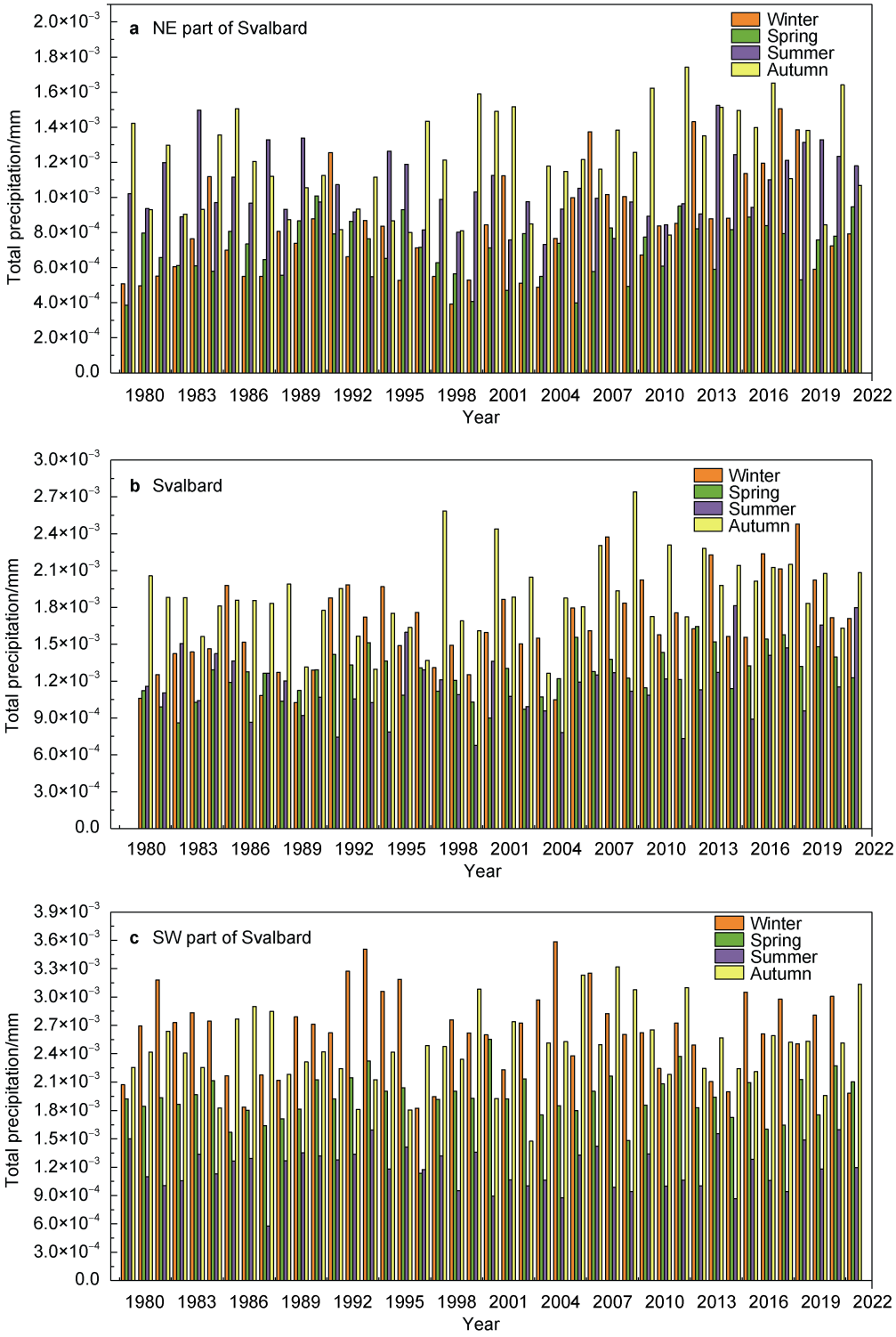

Figure 4 Precipitation over northeast part of Svalbard (**a**), Svalbard (**b**) and southwest part of Svalbard (**c**) for winter, spring, summer, and autumn for the span 1979–2021.

1.21×10^{-3} m. Tremendous variation in spell is observed during summer with significant highs and lows, irrespective of the range being very low and the average value being slightly lower than that during autumn (1.04×10^{-3} m). Winter precipitation variability, which was low over the previous span, is seen to peak during the recent span. The seasonal precipitation has an average value of 8.27×10^{-4} m, which is slightly higher than that during spring with an average value of 7.03×10^{-4} m.

When compared to the NE part of Svalbard, the landlocked Svalbard region (Figure 4b) has a maximum value of 2.7×10^{-3} m. The Svalbard precipitation range is slightly higher than that over the NE part of Svalbard, with values ranging from 0 to 2.7×10^{-3} m. Over Svalbard, the seasonal distinction in precipitation is seen to be slightly low. The average precipitation during winter, spring, summer, and autumn is 1.64×10^{-3}, 1.26×10^{-3}, 1.17×10^{-3} and 1.90×10^{-3} m, which means all the spells received during each season are almost the same. Finally, over the SW part of Svalbard, the precipitation ranges from 0 to 3.6×10^{-3} m, which is the highest compared to the other two areas of interest. The spell is strongest in winter, followed by autumn, spring, and finally summer. Average winter precipitation is 2.63×10^{-3} m, which is maximum when compared to seasons, autumn, spring and winter which has an average value of 2.46×10^{-3}, 1.92×10^{-3} and 1.18×10^{-3} m, respectively.

Figure 4 shows that the south is becoming increasingly wet (maximum 0.05 mm·(10 a)$^{-1}$, p<0.1) while the north is becoming drier (minimum –0.03 mm·(10 a)$^{-1}$, p<0.1). Time series of annual precipitation show only a weak (not significant) positive trend of 0.005 mm·(10 a)$^{-1}$ (p>0.1). If the precipitation is primarily in the form of rain, the mean precipitation distribution shown in Figure 4 is most pronounced over the SW coastal regions (0.24 mm·a^{-1}), while rainfall is nearly absent in the NE, which could be the cause of such trends. This pattern illustrates a negative trend at low elevations, due to lower summer precipitation rates, and a substantial increase in rainfall at high elevations due to higher temperatures. Although the analysis of extreme precipitation events in Svalbard reveals no significant trend over the most recent decades when compared to the past decades, the variable as a whole cannot be neglected. Researchers in the past have already reported the decline of spells around the region and have named the region "the polar desert" (Bintanja et al., 2018) (mostly Arctic). The importance of precipitation over the domains is clearly stated in such documentation.

4.3 Variability in wind patterns

Figure 5 reveals wind direction and wind speed over the considered domains (NE of Svalbard, Svalbard, and SW of Svalbard) during the years 1979–2021 (42 years). Each colour in the figure represents the speed at which the wind is seen blowing over the considered domain for the four seasons: winter, spring, summer, and autumn. Figures 5a, 5b, 5c, and 5d represent wind speed and wind direction during the winter, spring, summer, and autumn seasons over the NE part of Svalbard. Figure 5a clearly shows that the majority of the winds are directed from the south during the winter. The wind speed range is seen to be between 5.5 and 10.4 m·s^{-1}. Many of them lie within the range of 7–9 m·s^{-1}. There is almost no wind from the south in the area. By spring (Figure 5b), the range of wind speed reduces to 4.3–8.5 m·s^{-1}. Unlike in the winter, the wind is seen to be present in all directions here, with a range of 6.8–7.7 m·s^{-1}. Wind speeds greater than 7.7 m·s^{-1} are only observed in the SE portion of the domain. During the summer (Figure 5c), the wind speed drops to 6.7 m·s^{-1}, which is also the maximum speed attained over the region during that season. Majority of the winds are found to be from the southern and SW directions of the area. By autumn (Figure 5d), the wind originates purely from the south (including SW and SE). By now the range has risen and varies between 5.4 and 9.3 m·s^{-1}. The area has very low wind from the northern parts of the considered region.

Figure 5e, 5f, 5g, and 5h show the wind speed and wind direction over Svalbard during winter, spring, summer, and autumn. During winter (Figure 5e), the wind speed varies from 5.6 to 8.9 m·s^{-1}. The northern portion is devoid of any wind. The majority of them originate from the south. Further in spring (Figure 5f) the pattern resembles that of the previous season (winter); however, the range of wind speed reduces to 1.4–7.8 m·s^{-1}. During summer (Figure 5g) the direction of the wind shifts more towards the SW direction, with wind speeds slightly lower, ranging from 3.3 to 5.5 m·s^{-1}. However, by autumn (Figure 5h) the shift in the direction is seen more towards the eastern side, with slightly higher wind speed values ranging from 4.6–8.4 m·s^{-1}. Finally, Figure 5i, 5j, 5k, and 5l show the wind rose diagram over the SW part of Svalbard during winter, spring, summer, and autumn. Figure 5i shows that the wind originates primarily from the east over this region, with wind speeds falling between 6.9 and 11.6 m·s^{-1}. The range of wind speeds in this area is the highest compared to any other region during this season. During spring (Figure 5j), the direction of the wind is the same as that of the previous season, but the range has slightly increased to 5.4–10.9 m·s^{-1}. However, by summer (Figure 5k), the wind originates from the south. Furthermore, during autumn, the wind shifts to the east (Figure 5l), with a range of 5.6 to 11.2 m·s^{-1}.

On average (majority points), it is found that the summer and winter wind directions are slightly different, yet they remain confined to the same sector in terms of the direction of the originating wind. Wind directions at higher pressure levels are thought to change dramatically with topography. In all the neighbouring regions of Svalbard, winds are mostly from the south. An important observation from the wind rose diagram is that the winds are extremely insignificant in the north, which would have been beneficial during the sea ice formation time. The northerly winds will

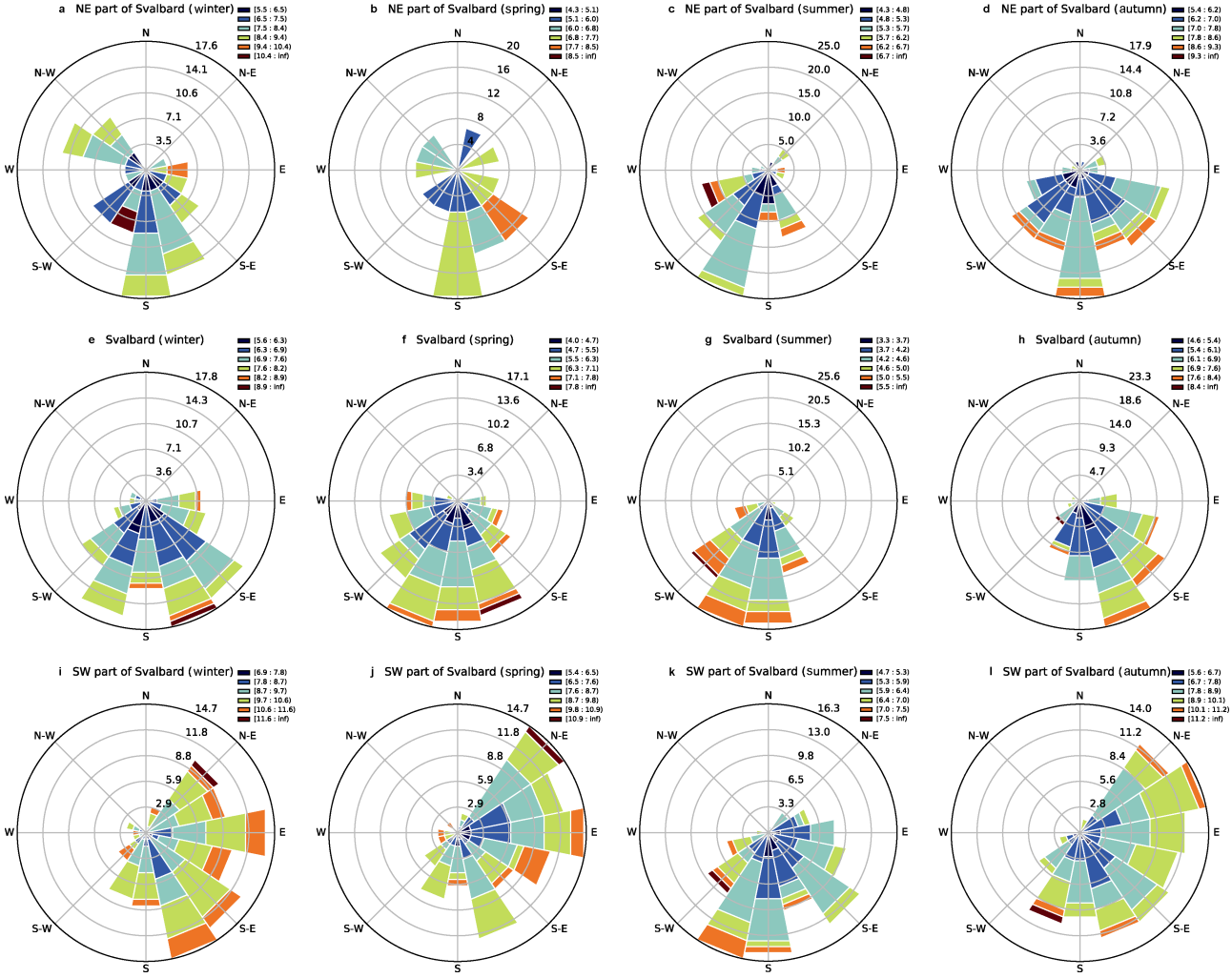

Figure 5 Wind rose ($m \cdot s^{-1}$) diagram of northeast part of Svalbard (**a–d**), Svalbard (**e–h**), and southwest part of Svalbard (**i–l**) of four seasons for the span 1979–2021.

most likely bring cold Arctic air over the region, and the relatively high wind speeds will result in significant heat loss from the ocean. It is hypothesised that these conditions along with other atmospheric conditions favoured the rapid growth of sea ice over areas with cold Arctic water already present. However, in this case, the majority of the winds are from the south, raising the possibility that they may carry warm air along with them, warming the nearby water bodies around Svalbard even during the winter.

4.4 Variability in SSS

The SSS profiles of the three regions during different seasons are illustrated in Figures 6a, 6b, and 6c. Over NE part of Svalbard (Figure 6a), the range of SSS lies between 16.60 and 19.45 PSU. The highest values are observed in spring, followed by winter, then summer, and finally autumn. In summer, the initial years until 1997 were found to be uniform, with values having an average of 18.92 PSU. Later, the values were seen to fluctuate tremendously, and the average post-1997 was 18.40 PSU. During spring, the variations remained constant until 2000, with an average value of 19.14 PSU, and as the years passed (after 2000), the average value fluctuated and fell to an average value of 18.75 PSU. However, during summer, the higher values remain confined to the year 1993, with an average value of 18.75 PSU; later, post-1993, the average value is seen varying and attaining lower average value of 17.97 PSU. By autumn, SSS is found to be significantly varying around lower values, with mean value of 18.30 PSU till 2000, and after 2000, it is found to be even lower, at 17.59 PSU. Over Svalbard, the variable SSS is found to vary between 13.06 and 15.41 PSU. The highest value of salinity is observed during winter, followed by spring, autumn, and finally summer. During winter, almost all the yearly averages until 2010 fall under the range of 14.8 PSU, whereas post-2010, the value increased to reach 15.07 PSU. By spring, the value of salinity is found to be tremendously high and is significantly visible from the plot Figure 6b. The average salinity over the 42-year period is 15.11 PSU. Later in summer, the values significantly drop. The average

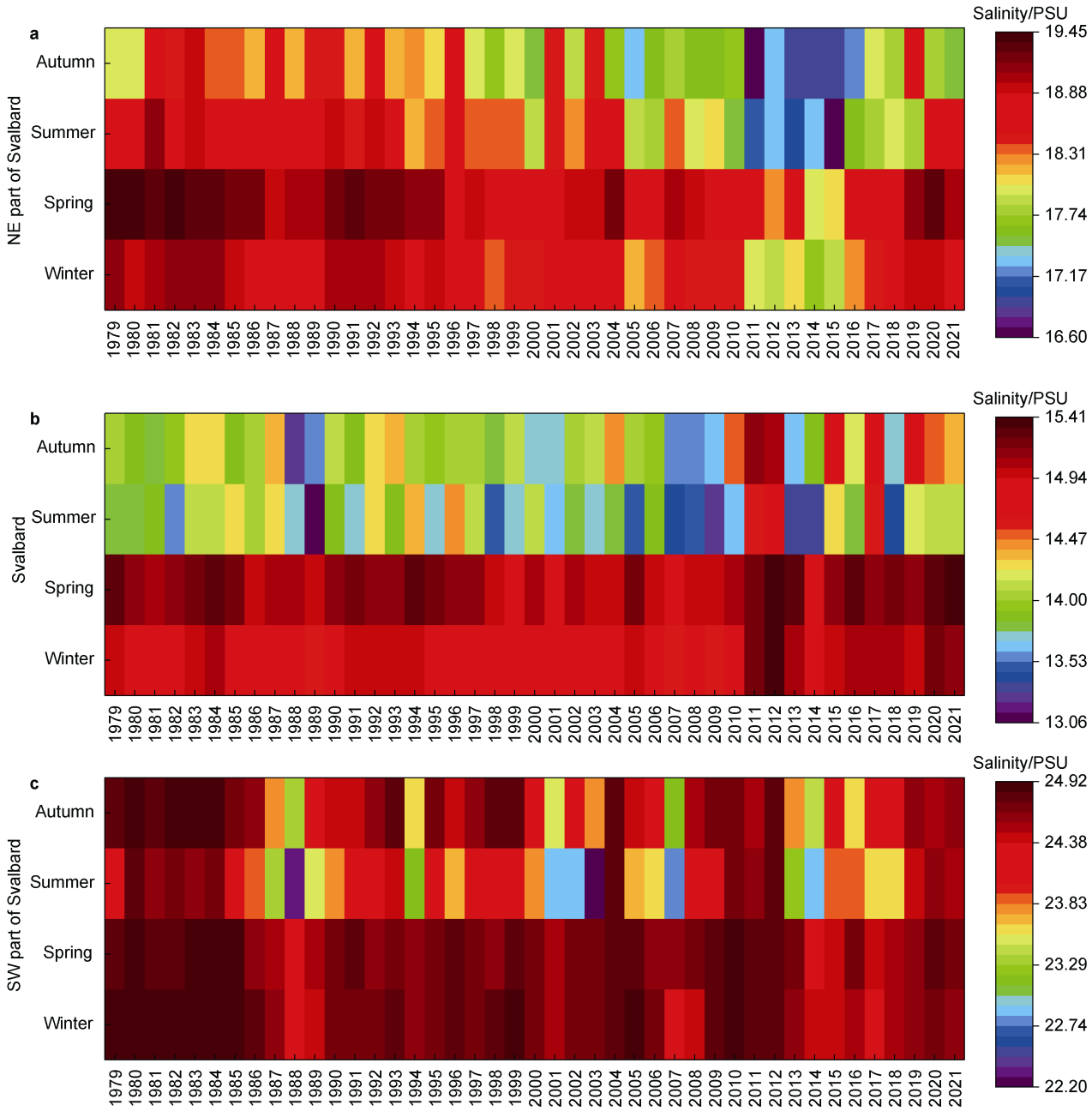

Figure 6 Hovmoller plots of sea surface salinity (SSS) in PSU averaged over space and time for the span for 1979–2021 over northeast part of Svalbard (**a**), Svalbard (**b**), and southwest part of Svalbard (**c**).

calculated shows just 13.88 PSU, indicating the salinity content over the sea during the particular season is the least compared to the aforementioned seasons discussed in the section. Further in autumn, the average is slightly higher, with all the plots lying closer to the average value of 14.09 PSU. Lastly, over the SW part of Svalbard, the range of salinity over the sea is found to be the highest compared to the NE part of Svalbard and Svalbard itself, indicating the sea over this area is highly saline in nature. The range lies between 22.20 and 24.92 PSU. Till 1985, the salinity of the sea remained constant in winter with a value of 24.85 PSU, after which the salinity profile was found to be fluctuating. The average of the salinity values post-1985 is 24.63 PSU, which is not much different from the previous quantity. The pattern is similar to that of winter in the spring, with an average value of 24.67 PSU. In summer, the yearly fluctuation is found to be significantly high. Finally, the autumn season also shows a similar trend to that of the summer, except for the fact that during the autumn, the values remain somewhat similar or constant during the initial phase. In the current study, understanding the SSS is important for two main reasons. First, along with temperature, salinity directly affects seawater density and, therefore, the circulation of ocean currents from the tropics to the poles. These currents

control how heat is carried within the oceans and ultimately regulate the world's overall climate. Second, SSS is intimately linked to earth's water cycle and to how much freshwater leaves and enters the oceans through evaporation and precipitation. Measuring salinity is one way to probe the water cycle in greater detail.

4.5 Variability in sea ice concentration

Between 1979 and 2021, the annual mean SIC in the SW of Svalbard, the NE of Svalbard, and Svalbard was 5.26%, 93.59%, and 34.07%, respectively. Ice is present during all months, with the lowest concentration in September (Figure 7). Highest ice concentrations are generally attained in March (Figure 7).

During the period 1981–1990 (Figure 7a), the NE part of Svalbard has ~100% SIC, while the region around Kvitøya (an island in the NE part of Svalbard) has SIC of 100%. Sections around Svalbard have all type of gradients. However, SIC is observed to be less than 71% in the southwest part of Svalbard. A small contouring of different SIC (in decreasing order) is observed over this portion. The intensity of SIC over the southwest of the country decreased between 1991 and 2000 (Figure 7b). The range lies almost below 29%. Additionally, no SIC is found below 72°N, which was not the case in the latter span. The plots represent the maximum month (March) of a year; therefore, it can be understood that the plots depicted show the maximum condition of sea ice prevalent over the region during the considered decade. The region around Kvitøya is seen to lose some sea ice, however, the portion near Greenland is seen to have intensified when compared with the previous decade. Around Svalbard, the intensity is quite high in the NE corner, and slightly lower in the SW corner when compared with 1981–1990. SIC, with a prevalence of 71%–85%, begins to appear around Kvitøya in the NE corner of Svalbard between 2001 and 2010 (Figure 7c). Over this span, the spatial distribution of SIC is considered to be constrained. However, the region near Greenland seems to be unchanged. In

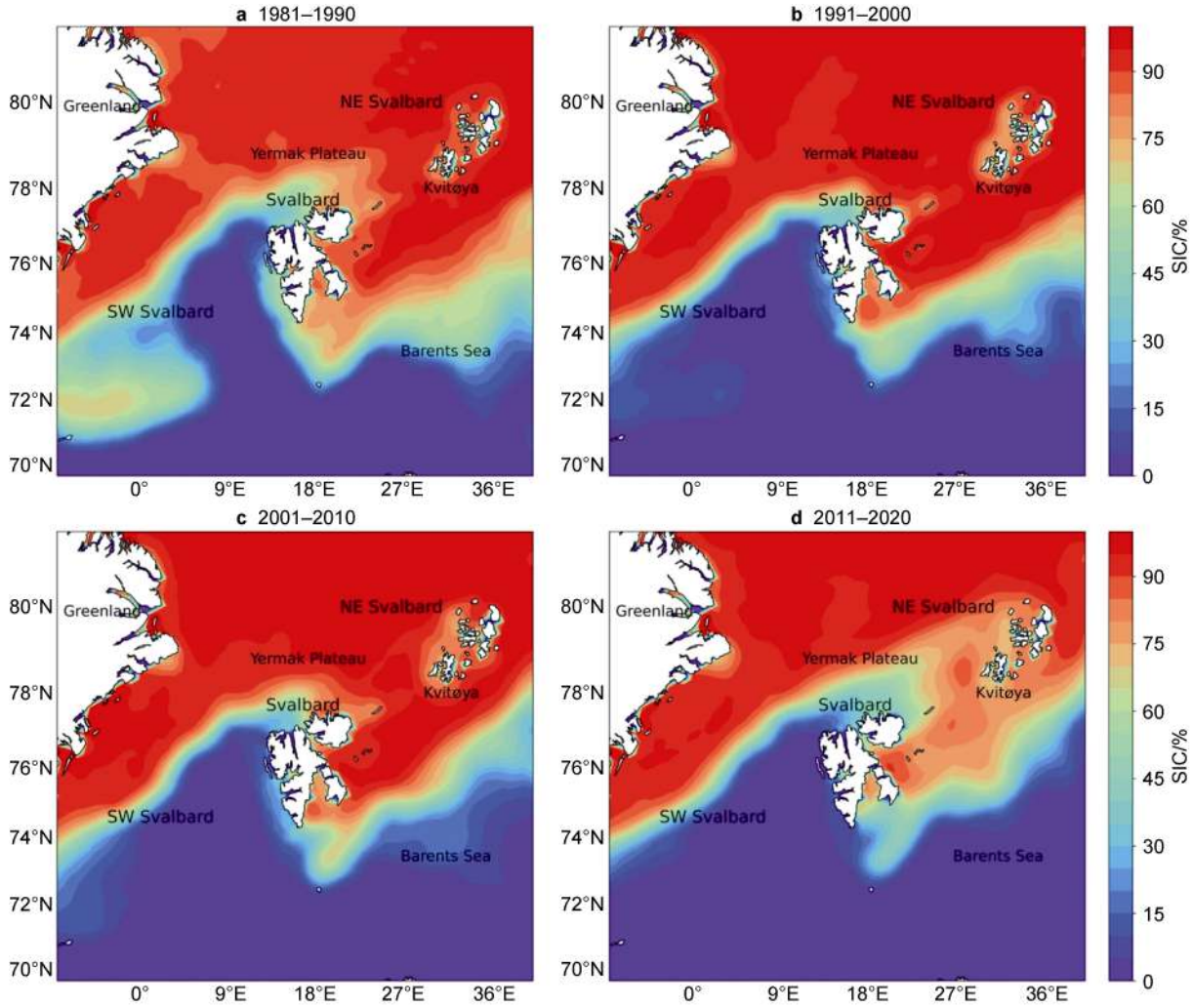

Figure 7 Inter-decadal variation in SIC over northeast part of Svalbard, Svalbard, and southwest part of Svalbard during maximum sea ice condition in March for years 1981–1990 (**a**), 1991–2000 (**b**), 2001–2010 (**c**) and 2011–2020 (**d**).

contrast to the previous three decades, SIC over the NE section has decreased significantly between 2011 and 2020 (Figure 7d). The observed SIC is seen to be below 100%, except for a few pixels in the north most corners that are very close to the Arctic Circle. Similarly, the portion around the Svalbard Archipelago has experienced tremendous sea ice loss during the recent decade. The change observed over the SW part of Svalbard is much more pronounced. It has been found to be almost ice-free. No sea ice is found below 72°N, which states that the region has undergone drastic melting. The freezing conditions this winter weren't enough for the lost sea ice to develop. Lower SIC have been gradually moving north and east along Svalbard's northern coast since the 1980s, as evident by the spatial winter ice loss north of Svalbard since the 1980s. By 2011–2020, a winter average SIC of 40% reaches almost 79°N east of our study region, reflecting the lowest winter ice minimum.

Figure 8 clearly demonstrates that SIC has decreased north of Svalbard over the last three decades, with a record low annual minimum in 2012 (not shown). Ice loss occurs in all months, with the greatest negative trends occurring in the winter (DJF). The resulting winter SIC loss is ~10%·(10 a)$^{-1}$. August and September demonstrate the smallest reductions. The summer SIC experiences an ice loss of ~6%·(10 a)$^{-1}$. Similarly, during the sea ice minimum condition (September), the spatial SIC is seen to have decreased with the passage of each decade (Figure 8). During the period 1981–1990 (Figure 8a), the NE part of Svalbard had SIC of 100% in the centre and towards the north, near the Arctic, surrounded by contours of lower SIC. The region to the north of Kvitøya is observed to have SIC of ~60% and to the south it is much lower (~15%). Around Svalbard Archipelago, there is not much ice in the SW direction. The archipelago is surrounded by sea ice with lower concentrations. Beneath 72°N, ice-free conditions exist over the southwest part of Svalbard. However, during the decade 1991–2000 (Figure 8b), the ice-free condition over SW portion of Svalbard starts below 74°N. That means almost the entire spatial domain is free of ice. And 100% of SIC is seen shifting towards the Greenland region during this span,

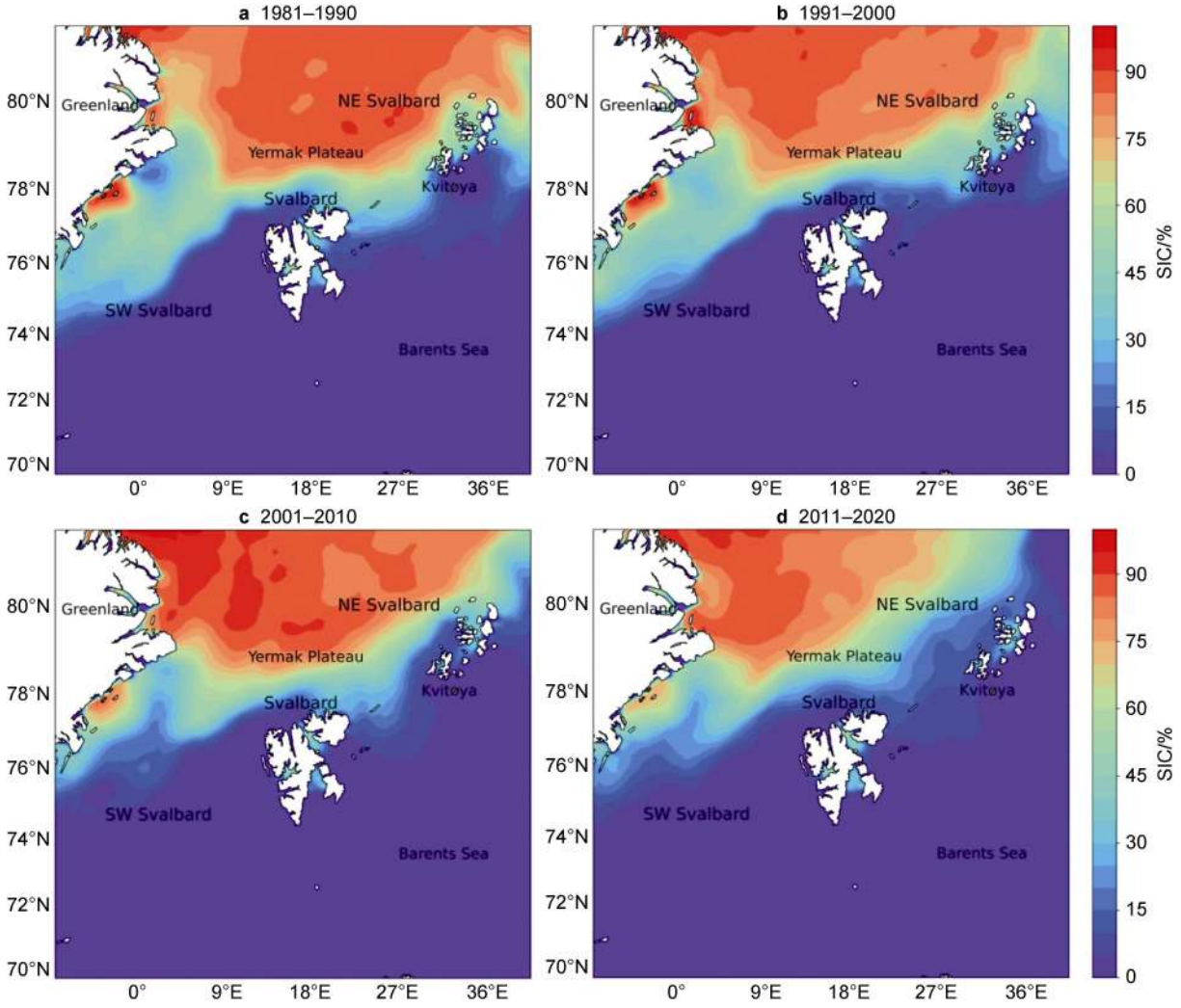

Figure 8 Inter-decadal variation in SIC over northeast part of Svalbard, Svalbard and southwest part of Svalbard during minimum sea ice condition in September for years 1981–1990 (**a**), 1991–2000 (**b**), 2001–2010 (**c**), and 2011–2020 (**d**).

making the NE portion of Svalbard fall in terms of SIC percentage; the observed SIC over the region is ~85%. Kvitøya doesn't have a dense concentration of sea ice in its vicinity. It is usually surrounded by SICs ranging from 71% to 100%. Except for some areas near Greenland, the region is almost devoid of concentrations greater than 90% by 2001–2010 (Figure 8c). The SW portion of Svalbard and Kvitøya is surrounded by 15% SIC. The recent decade, 2011–2020, has seen a much more dramatic change in SIC (Figure 8d). Here all the considered areas are dominant, with SIC below 29%. Overall, Figure 8 shows the evolution of the SIC from 1981 through 2020. Many features of the spatial structure of the residual term are conserved over the period; for example, the Yermak Plateau stands out as a regional maximum of sea ice loss during all four decades. However, there has also been some interesting evolution over the period. In particular, the region of SIC loss appears to expand eastward along the Atlantic Water Boundary Current in the Arctic Ocean pathway, from north of Spitsbergen in the 1980s, past the study region in the 1990s and 2000s, to north of Franz Josef Land in the 2010s (not shown, but observed during the course of study).

An attempt has been made to statistically validate the SIC data retrieved for various regions. Mean, standard deviation, skewness, kurtosis, and slope of the averaged SIC over almost four decades (1979–2021) over the three considered domains, SW of Svalbard, NE of Svalbard, and Svalbard, for the years 1979–2021 (42 years), are represented in Table 2. The mean SICs for the NE part of Svalbard, Svalbard, and the SW part of Svalbard are 93.59%, 34.07%, and 5.26%, respectively. The values suggest that the SIC increases as one moves towards the north, which is as expected considering the closeness of these areas to the Arctic Circle (as lesser sunlight is received with increase in latitude). The standard deviation, which represents the deviation of SIC from the mean values, shows a higher value for Svalbard than for NE and SW. Skewness reveals that SIC across all regions is highly skewed, as the values in Table 2 are less than –1 or greater than 1. The kurtosis values over NE, Svalbard, and SW are 12.58, –1.30, and 8.39, respectively. As the values for NE and SW are highly positive, it indicates that the value of SIC is more present at the tail than at the mean value. Finally, the slope value over each region indicates the rise or fall of SIC. Svalbard has a slope of –0.60, then NE has a slope of –0.41, and finally SW has a slope of –0.32. The negative sign of the slope indicates that these values are falling with the passage of time. The amount of SIC reduces with the passage of each year.

Table 2 Mean, standard deviation, skewness, kurtosis and slope of averaged SIC over NE of Svalbard, Svalbard and SW of Svalbard, during 1979–2021

	NE of Svalbard	Svalbard	SW of Svalbard
Mean value of SIC/%	93.59	34.07	5.26
Standard deviation/%	14.60	20.91	10.57
Skewness	–3.37	–0.29	2.89
Kurtosis	12.58	–1.30	8.39
Slope	–0.41	–0.60	–0.32

Seasonal variations of SIC over the considered regions are displayed in Figure 8. In the spring, sea ice is found to be highly fluctuating over SW Svalbard (Figure 9a). However, the variation is only confined to 2003. During winter, a similar trend is witnessed. From the observations, it can be understood that the fluctuation in the SIC is highly dominant in the past 20 years compared to the recent 20 years. During summer and autumn, the range of the SIC remains confined to 0–10%. After 2000, it was observed that during these seasons the annual average concentration did not reach above 10%. The *y*-axis of SIC clearly shows that the range of concentration reaches only up to 60%, and that too for a limited time span, making the region highly vulnerable to sea ice melting. The recent trend clearly shows that the region will be ice-free soon.

Over the NE of Svalbard (Figure 9b), the trend is completely opposite. Here, higher fluctuations are observed for greater SIC values. Over this region, high variation in SIC is observed during the summer and spring seasons, and this fluctuation is seen to be rising with the passage of time (years). During winter and spring, the SIC is 100%, giving favourable conditions for the sea ice to grow. However, after 2010, during the recent decade, it was found that the range of SIC during winter was also varying. During the same time period, the autumn SIC is seen to fall and sometimes fall below 10%. Perhaps the very neighbouring regions of the Svalbard Archipelago (Figure 9c) show a distinct trend from the other two regions. Here each seasonal variation can be distinctly identified. The total range of SIC over the area is around 0–70%. No significant SIC is observed at 100%. Winter and spring have the highest SIC, while autumn has the lowest.

Overall, the observed annual mean SIC at the study sites (averaged over all three regions) from 1979 to 2021 (42 years) shows that SIC declined sharply during 2010–2020 relative to the three previous decades. This is also evident when considering the decadal mean SIC and the decadal standard deviation (SD) of the annual average SIC. In the 2010s, mean is 45.50% and the SD is 22.61%, compared to the 1980s, where the mean is 77.90% and the SD is 12.87%. In the 1990s, the mean is 74.76% and the SD is 7.6%; in the 2000s, the mean was 67.97% and the SD is 12.87%. In 2012, 2013, 2016, and 2018, the annual mean SIC is below 40%, lower than any year between 1979 and 2010. This change was due to reduced SIC in both February–July and August–January. During the preceding three decades, the area was largely ice-covered in the spring, with a mean February–July SIC greater than 75% during all years except 2006. Autumn SIC declined in the 2000s, but only once (1984) during 1980–2010 did August–January SIC fall below 10% (as opposed to 5 out of 10 years after 2010), when averaged over the entire considered regions. The major cause of such sea ice loss found recently is due to the

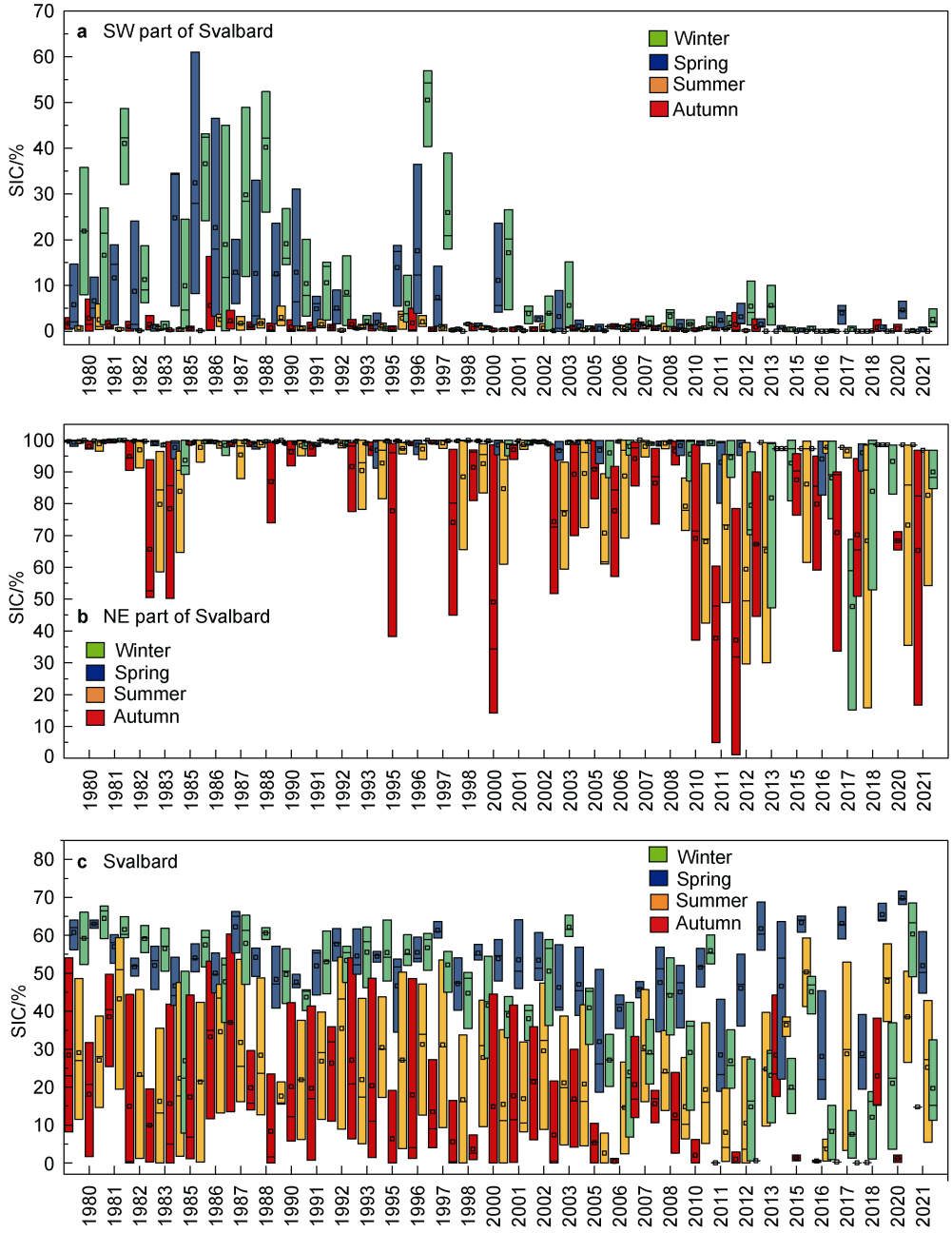

Figure 9 Seasonal SIC whisker plots during winter, spring, summer and autumn over southwest part of Svalbard (**a**), northeast part of Svalbard (**b**), and Svalbard (**c**) for the span 1979–2021.

formation of thin ice, which can no longer withstand the hot summer. The inability of sea ice to form thicker ice may be due to a variety of atmospheric factors, as discussed in previous sections. However, in the upcoming section, each atmospheric variable is being statistically correlated with SIC to understand the influence of each on the sea ice condition over the considered regions.

4.5.1 Role of atmospheric and oceanic factors in sea ice loss

The summer sea ice decrease was caused by the feedback process of the atmosphere, as the sea ice formation in winter was mainly determined by the amount of heat the ocean received. The interplay of atmospheric and oceanic factors, including temperature, precipitation, wind speed, and SSS, on sea ice loss is discussed in this section. The correlation matrices are calculated to identify the links between SIC and other parameters (temperature, precipitation, wind speed, and SSS) for the NE part of Svalbard, Svalbard, and the SW part of Svalbard (Table 3). The results indicate a significant negative correlation ($p \leqslant 0.05$) between SIC and temperature, whereas other parameters, such as precipitation, wind speed, and salinity, have a significant positive correlation with SIC in some seasons (Table 3).

Table 3 Correlation matrix of the seasonal average (1979–2021) of sea ice concentration (SIC) with air temperature (AT), precipitation (PPT), wind speed (WS) and sea surface salinity (SSS) over NE part of Svalbard, Svalbard and SW part of Svalbard (the numbers are statistically significant at a confidence level of 95%)

Region	Correlation	Winter	Spring	Summer	Autumn
NE of Svalbard	$r_{(SIC, AT)}$	–0.57	–0.18	–0.16	–0.40
	$r_{(SIC, PPT)}$	–0.58	–0.17	–0.09	–0.23
	$r_{(SIC, WS)}$	–0.36	–0.13	–0.08	0.06
	$r_{(SIC, SSS)}$	0.36	0.35	0.44	0.48
Svalbard	$r_{(SIC, AT)}$	–0.84	–0.38	–0.24	–0.44
	$r_{(SIC, PPT)}$	–0.56	–0.39	0.04	–0.19
	$r_{(SIC, WS)}$	–0.09	–0.20	–0.02	–0.13
	$r_{(SIC, SSS)}$	–0.27	0.07	0.22	–0.28
SW of Svalbard	$r_{(SIC, AT)}$	–0.66	–0.37	–0.48	–0.48
	$r_{(SIC, PPT)}$	–0.41	–0.23	0.07	0.13
	$r_{(SIC, WS)}$	–0.36	–0.12	–0.09	0.11
	$r_{(SIC, SSS)}$	0.00	0.15	–0.09	0.17

Temperature and SIC have stronger correlations than other factors in the NE part of Svalbard, indicating that temperature changes have a significant impact on sea ice (Table 3). The albedo influences the outgoing and incoming solar radiations, thereby increasing the incoming radiations and causes a further increase in the temperature above it (Zhang et al., 2018). In the NE Svalbard sector, the variability of SIC was rather low because the presence of thicker ice. SIC is seen decreasing during the summer due to atmospheric positive feedback (as found that temperature is increasing, precipitation is increasing, winds from the south are predominantly strong, and salinity is decreasing).

However, the highest negative correlation between temperature and SIC value is observed during the winter season (r=–0.57). Precipitation and wind are also found to have a negative influence on SIC, with r values of –0.58 and –0.36, respectively. However, with SSS, it has a positive association (r=0.36). To understand the trend during the winter season, as it is also the season when sea ice begins to thicken, the temporal profile of SIC along with atmospheric and oceanic variables are depicted in Figure 10. Figure 10 depicts how SIC gradually declines after 2000. However, parameters like air temperature, precipitation, and wind speed are found to increase over the region. The slopes, of all the considered atmospheric parameters are slightly inclined in the upward direction. However, SSS shows patterns that overlap with those of SIC. After 2000, SSS showed a downward trend. A general picture of the intertwined relationship between atmospheric and cryospheric parameters can be seen here. Furthermore, the negative correlation between air temperature, precipitation, and wind speed persists during the spring and autumn seasons. However, during autumn, the association of wind speed and SIC becomes slightly positive, with r=0.06. For every season, salinity remains positive, reaching its highest value during autumn with r=0.48. It is understood that when sea ice forms, the water's salinity increases as salt is ejected into the ocean during the freezing of the ice. During winter, the highest negative correlation between air temperature and SIC is observed over Svalbard, with a value of r =–0.84 (Table 3). Further, the value decreases to –0.38 from –0.24 as the seasons progress from spring to summer. Similarly, precipitation is also found to be highly negative during winter (r=–0.56) compared to any other season in this region. While observing the temporal profiles of these parameters (Figure 10) not much variation is observed in the precipitation or wind speed. However, significant winter warming is also observed. Post 2005, salinity is seen to reach higher values, indicating that there are more ice freeze-ups. But, SIC clearly indicates a downward fall after 2005. Over the SW part of Svalbard, too, the decrease in SIC mainly occurs due to the temperature of the air above it (r=–0.66) during winter, as evident from the correlation matrix in Table 3. From the discussions in the previous sections, it is now understood that the sea ice over this region is generally thin. Even in summer, when sea ice is thinning, the small heat promotes melting and results in a decrease in SIC (r=–0.49). Among the three regions, the correlation between SIC and precipitation, wind speed, and SSS for the SW section is the lowest ($|r|$<0.5). However, precipitation and wind speed are observed to have a low correlation in all seasons. As it is often observed that increase in precipitation is often associated with increased wind speed, this implies convergence feedback by which evaporation induces moisture convergence that feeds increases in precipitation. Figure 10 shows that SIC drops gradually after 2000, while air temperatures rise dramatically. Additionally, precipitation and wind speed are found to behave in a similar fashion, with only slight variations in salinity patterns.

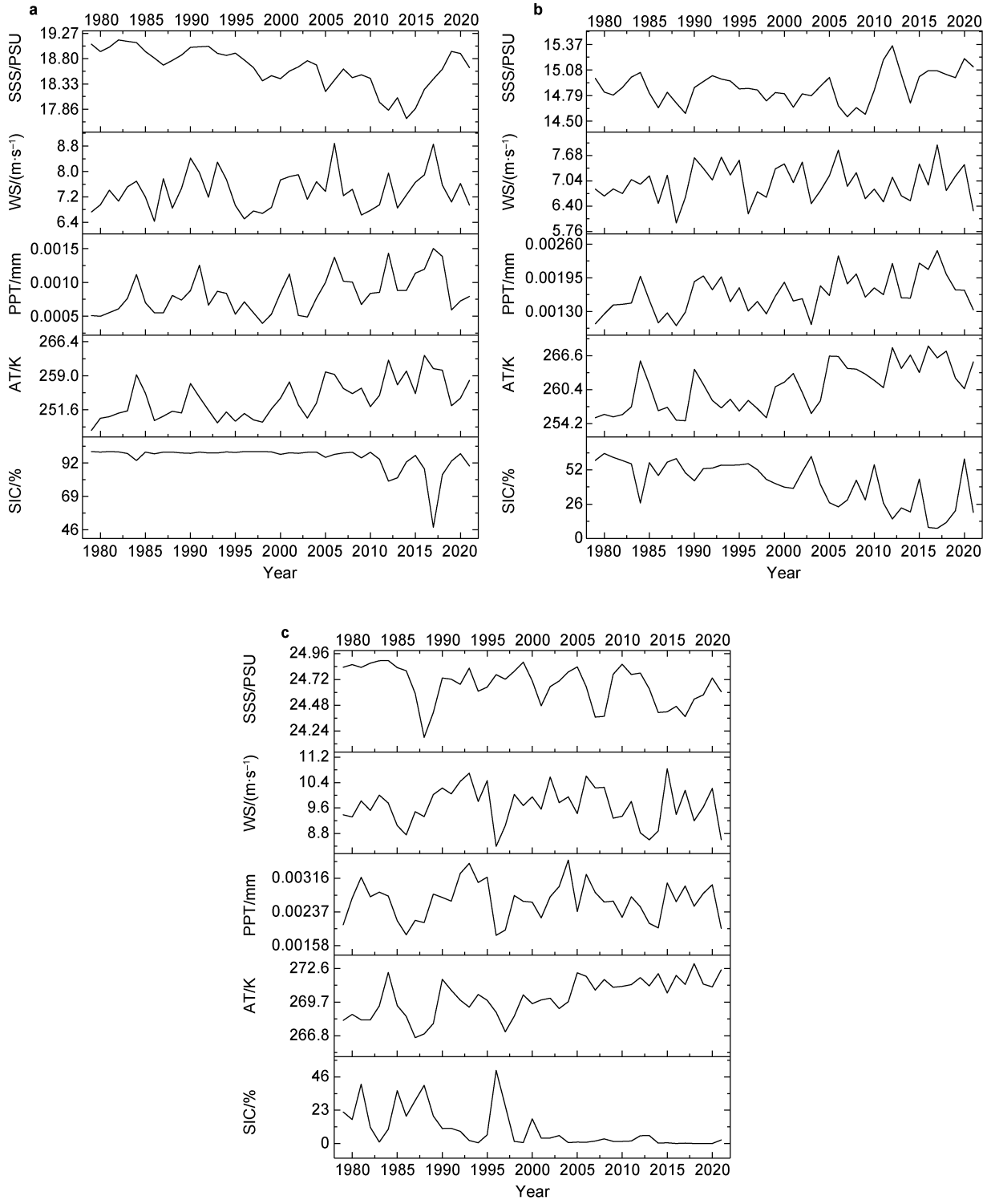

Figure 10 Time series of sea ice concentration (SIC), air temperature (AT), precipitation (PPT), wind speed (WS) and sea surface salinity (SSS) for the span for 1979–2021 over northeast part of Svalbard (**a**), Svalbard (**b**), and southwest part of Svalbard (**c**).

Table 3 shows that the decrease in winter sea ice is greater than the decrease in summer sea ice. It indicated that the increase in temperature in winter may have contributed to the sharp decrease in winter SIC for the NE and SW of Svalbard during the past several decades. The presence of warm water over the region is one of the well-known factors responsible for low sea ice conditions. These warm waters are the major contributor to the ice loss during large winter ice reductions. With winter air temperatures well below freezing, the Atlantic water is the only heat source in the area

north of Svalbard (Rudels, 2010), and its influence is expected to be greatest during the winter. During summer, other factors probably contribute more to the observed ice loss. Warmer surface waters delay ice formation, resulting in lower ice concentrations in early winter. As the SW and NE of Svalbard continue to warm and the ice cover continues to decrease, a number of key elements remain almost unobserved. This study has so far documented the warming in both the atmosphere and ocean, which has caused a decline in ice concentration since 1979. The long-term forecasts for sea ice over Svalbard are horrifying, especially for the winter ice (Hansen et al., 2013). This is already revealed by the correlation value between SIC and temperature over Svalbard during winter (r=–0.84) in Table 3. The large loss of the winter ice north of Svalbard is not typical for other regions inside the Arctic Ocean but more in line with the on-going changes in the Barents Sea over the last decades. Now that the Atlantic waters heat transport seems to have reached an all-time high in 2004, a recovery of the winter ice can only be expected over the next 10 years (Årthun et al., 2012).

4.5.2 Linear regression analysis of SIC with atmospheric parameters

Apart from the correlation indices discussed in the aforementioned section, here linear regression analysis is performed between the cryospheric parameter (SIC) and atmospheric parameters (AT, PPT, WS, and SSS) over the NE part of Svalbard, Svalbard, and the SW part of Svalbard and is depicted in Figure 11. SIC and AT own a high linear correlation and also have noticeable seasonal variation characteristics over the region during winter (Figure 11a). When AT increases, SIC decreases, and vice versa. Over Svalbard during winters, $r^2_{(SIC, AT)}$=0.71 (p<0.05), indicating a strong relationship between the two quantities. At higher SIC, a clustering of points is observed, indicating that the probability of sea ice occurrence is greater when the temperature is at its lowest. In the case of Svalbard, SIC typically increases in the winter months as temperatures drop. Further, Figure 11b shows the relationship of SIC and PPT over Svalbard during winter season. From the r^2 value of 0.32, it is evident that the relationship between SIC and PPT over Svalbard in winter is not straightforward and can be influenced by various factors. Generally, it is known that precipitation is mostly in the form of snow, which can contribute to the growth of sea ice by adding freshwater to the surface of the ocean, which can lower the freezing point of seawater and facilitate the formation of sea ice. However, heavy precipitation events can also lead to a decrease in SIC by creating a layer of insulating snow on top of existing sea ice, which can prevent the ice from thickening and expanding, which may be the situation in the considered case (region) (Kalnay et al., 1996). However, in the case of wind speed, majority of it is found occurring at lower SIC (Figure 11c). The r^2 value between these two variables is 0.13, which

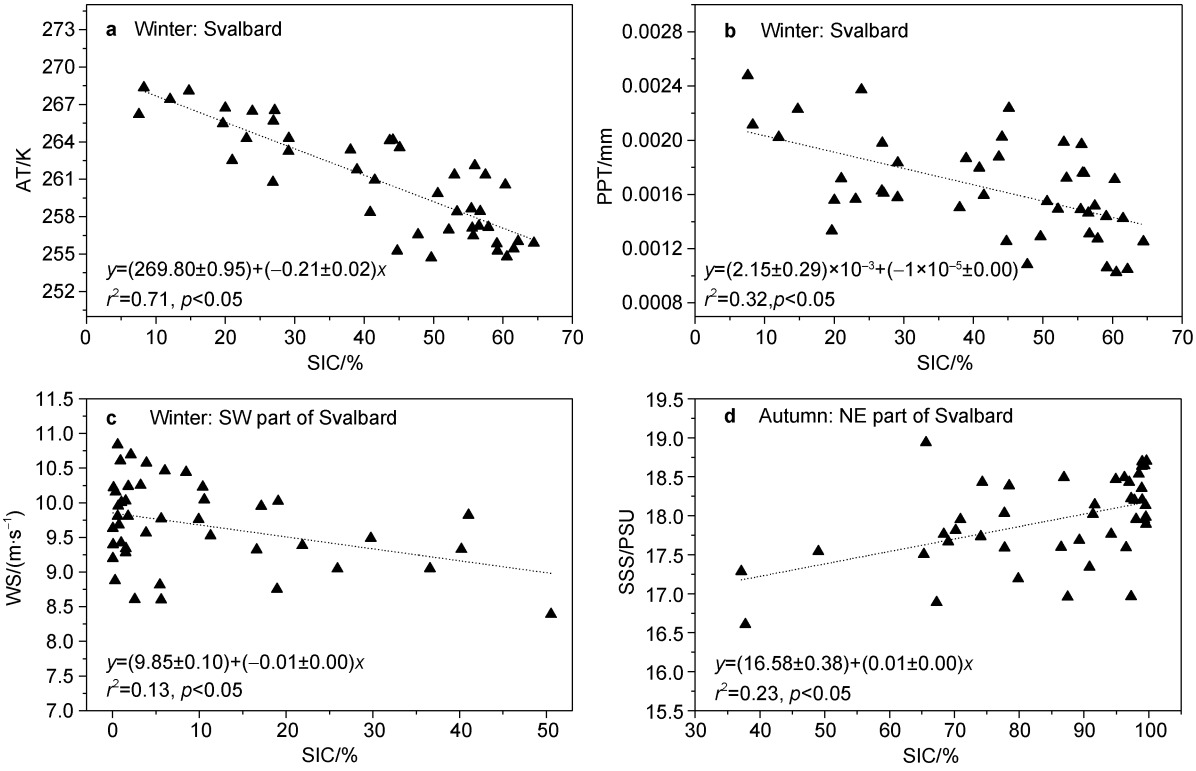

Figure 11 Linear regression analysis of sea ice concentration (SIC) with atmospheric parameters air temperature (**a**), precipitation (**b**), wind speed (**c**), and sea surface salinity (**d**).

doesn't provide enough information to state whether the wind has positive feedback or negative feedback on the sea ice condition. Wind speed can play a significant role in determining the distribution and extent of sea ice. Strong winds from the north can cause sea ice to move southward and out of the region, while weak or variable winds can allow sea ice to accumulate and thicken. Similar to wind speed, the role of salinity on SIC is also tough to determine (Figure 11d). The r^2=0.23, p<0.05, indicates that the relationship between the two is not significantly justifiable. It is understood that sea ice formation and growth are affected by salinity, as the freezing point of water decreases as salinity increases. Thus, higher salinity levels can lead to a decrease in SIC, as the water is less likely to freeze (Dee and Uppala, 2009). Conversely, lower salinity levels can lead to an increase in SIC, as the water is more likely to freeze. Salinity levels can be affected by several factors, including freshwater input from rivers and precipitation, as well as ocean currents and mixing. These factors can influence the distribution and extent of sea ice in the region.

5 Conclusions

The seasonal and regional variability of SIC with respect to changing atmospheric and oceanic conditions during 1979–2021 (42 years) was analysed based on the long-term satellite data which is the key highlight of the paper. All months experience an ice loss, with largest negative trends in December, February, and January (winter season). The resulting winter SIC loss is ~10%·(10 a)$^{-1}$. August and September demonstrate the smallest reductions. The summer SIC experiences an ice loss of ~6%·(10 a)$^{-1}$. The large-scale warming in the Arctic during the latest decades is also reflected in the regions around Svalbard.

During the considered span, winter temperatures have a growth rate of 0.23, 0.01, and 0.02 K·a^{-1} over the NE part of Svalbard, Svalbard, and the SW part of Svalbard, respectively. However, the rate of growth of the temperature during summer is seen to be 0.02, 0.04, and 0.01 K·a^{-1} over the aforementioned domains. From 1985 to 1990, 1991 to 1996, 1997 to 2002, 2003 to 2008, 2009 to 2014, and 2015 to 2020, the region NE of Svalbard experienced temperature rises of 0.38, –0.56, 0.58, 1.23, 0.62, and 0.20 K·a^{-1}, respectively. Whereas Svalbard experiences temperature rates of 0.21, 0.10, 0.49, 1.13, 0.59, and 0.21 K·a^{-1} from 1985 to 1990, 1991 to 1996, 1997 to 2002, 2003 to 2008, 2009 to 2014, and 2015 to 2020 respectively, and finally, the SW part of Svalbard experiences rates of –0.23, 0.49, –0.21, 0.61, 0.18, and 0.04 K·a^{-1} from 1985 to 1990, 1991 to 1996, 1997 to 2002, 2003 to 2008, 2009 to 2014, and 2015 to 2020 respectively. Overall, the increasing temperature trend has always affected the sea ice condition in a negative manner ($r^2_{(SIC, AT)}$=0.71, p<0.05). Trends in precipitation also reveal increasingly wet conditions in the south and drier conditions in the north, with a maximum of 0.05 mm·(10 a)$^{-1}$ and –0.03 mm·(10 a)$^{-1}$ (p<0.1), respectively. However, annual precipitation shows only a weak (insignificant) positive trend of 0.005 mm·(10 a)$^{-1}$, p>0.1. If the precipitation is predominantly in the form of rain, then the mean distribution of precipitation is most pronounced over the coastal regions of the SW (~0.24 mm·a^{-1}), while rainfall is nearly absent in the NE. Ultimately, the spell is strongest in winter, followed by autumn, spring, and finally summer. Winter precipitation totals 2.63×10^{-3} m on average. The seasons of autumn, spring, and winter have an average value of 2.46×10^{-3}, 1.92×10^{-3} and 1.18×10^{-3} m, respectively. The regression analysis (r^2=0.32, p<0.05) performed also states that the relationship between the two entities is negative in certain parts of Svalbard.

Based on the seasonal division, wind speeds are maximum during the autumn, decrease subsequently through the summer and spring, and are lowest during the winter. The wind direction in all the neighbouring regions of Svalbard is mostly from the south. Very low northerly winds are well established over the study area. The wind speed range is seen to be between 4.3 and 10.4 m·s^{-1}, with many falling within the 7–9 m·s^{-1}, range over the NE part of Svalbard. The wind speed over Svalbard ranges from 3.3 to 8.9 m·s^{-1}, and in the SW part of Svalbard ($r^2_{(SIC, WS)}$=0.13, p<0.05), it ranges from 4.7 to 11.6 m·s^{-1}. Winds were extremely insignificant in the north, which would have been beneficial during the formation of sea ice. The northerly winds will most likely bring cold Arctic air over the region, with relatively high wind speeds and a high heat loss from the ocean. However, in this case, the strongest winds are from the south, raising the possibility that warm air will be carried along, warming nearby water bodies around Svalbard even during the winter. Year-to-year sea ice variability is substantial, with winter means ranging between 10% and 90%. Although the winds seemingly do not have an impact on the trends, they have a significant impact on the year-to-year variability. Low values in SIC are consistently associated with winds from the south (fewer winds from the N), warmer air, and greater Atlantic water temperatures.

Further, the SSS profiles of the three regions during different seasons are also investigated. Over the NE part of Svalbard ($r^2_{(SIC, SSS)}$=0.23, p<0.05), the summer averages fall under 18.92 PSU; over Svalbard, they are found to vary between 13.06 and 15.41 PSU. Lastly, over the SW part of Svalbard, the range of salinity over the sea is found to be the highest compared to the NE part of Svalbard and Svalbard itself, indicating the sea over this area is highly saline in nature. The range lies between 22.20 and 24.92 PSU. The knowledge of SSS enhances the understanding of ocean currents from the tropics to the poles. These currents control how heat is carried within the oceans and ultimately regulate the world's overall climate. The temporal profile developed in the paper is also useful to the scientific community in terms of understanding the weightage of atmospheric and oceanic variables on cryospheric features.

During the past 42 years, there have been evident seasonal and regional differences for sea ice change around

Svalbard under the influence of sea ice export and atmospheric factors, and investigating them is the chief uniqueness of this paper. Hence, the atmospheric and oceanic factors should be better valued by distinguishing between the periodic influences and trends in future work. The results improve our understanding that the impact of SIC decline on the Svalbard climate is vital and is an important parameter for improving the predictions of sea ice and climate change in the Arctic as a whole.

Acknowledgement The authors immensely thank NSIDC NCEP/ NCAR, Reanalysis 1, GPCC and ERA-Interim reanalysis for making their datasets freely available.

Discloser Statement The authors declare that they have no conflict of interest.

Author contributions Dency V Panicker: visualization, methodology, software, data curation and original draft preparation. Bhasha Vachharajani: conceptualization, visualization, investigation and editing. Rohit Srivastava: conceptualization, visualization, investigation and editing.

References

Årthun M, Eldevik T, Smedsrud L H, et al. 2012. Quantifying the influence of Atlantic heat on Barents Sea ice variability and retreat. J Clim, 25(13): 4736-4743.

Bintanja R, Katsman C, Selten F. 2018. Increased Arctic precipitation slows down sea ice melt and surface warming. Oceanography, 31(2): 118-125, doi:10.5670/oceanog.2018.204.

Bintanja R, Selten F M. 2014. Future increases in Arctic precipitation linked to local evaporation and sea-ice retreat. Nature, 509(7501): 479-482, doi:10.1038/nature13259.

Bintanja R, van der Linden E C. 2013. The changing seasonal climate in the Arctic. Sci Rep, 3: 1556, doi:10.1038/srep01556.

Cavalieri D J, Parkinson C L, Gloersen P, et al. 1996. Sea ice concentrations from Nimbus-7 SMMR and DMSP SSM/I-SSMIS Passive Microwave Data, 1980–1999, National Snow and Ice Data Center.

Dee D P, Uppala S. 2009. Variational bias correction of satellite radiance data in the ERA-Interim reanalysis. Q J Royal Meteorol Soc, 135(644): 1830-1841, doi:10.1002/qj.493.

Førland E J, Hanssen-Bauer I, Nordli P. 1997. Climate statistics and longterm series of temperature and precipitation at Svalbard and Jan Mayen. Norwegian Meteorological Institute Klima Report, 1997, 21: 72.

Gerland S, Hall R. 2006. Variability of fast-ice thickness in Spitsbergen fjords. Ann Glaciol, 44: 231-239, doi:10.3189/172756406781811367.

Haas C, Lobach J, Hendricks S, et al. 2009. Helicopter-borne measurements of sea ice thickness, using a small and lightweight, digital EM system. J Appl Geophys, 67(3): 234-241, doi:10.1016/j.jappgeo.2008.05.005.

Hansen E, Gerland S, Granskog M A, et al. 2013. Thinning of Arctic Sea ice observed in Fram Strait: 1990-2011. J Geophys Res Oceans, 118(10): 5202-5221, doi:10.1002/jgrc.20393.

Hanssen-Bauer I, Førland E J, Hisdal H, et al. 2019. Climate in Svalbard 2100 – a knowledge base for climate adaption. NCCS report.

Hanssen-Bauer I, Førland E J. 1998. Long-term trends in precipitation and temperature in the Norwegian Arctic: can they be explained by changes in atmospheric circulation patterns? Clim Res, 10: 143-153, doi:10.3354/cr010143.

Holland M M, Stroeve J. 2011. Changing seasonal sea ice predictor relationships in a changing Arctic climate. Geophys Res Lett, 38(18): L18501, doi:10.1029/2011GL049303.

IPCC. 2021. Climate change 2021: the physical science basis. Cambridge, UK: Cambridge University Press.

Ivanov B V. 2019. Comparing the «earlier» and the «modern» warming in West Arctic on example of Svalbard. IOP Conf Ser: Earth Environ Sci, 231: 012023, doi:10.1088/1755-1315/231/1/012023.

Kalnay E, Kanamitsu M, Kistler R, et al. 1996. The NCEP/NCAR 40-year reanalysis project. Bull Amer Meteor Soc, 77(3): 437-471, doi:10.1175/1520-0477(1996)077<0437: tnyrp>2.0.co;2.

Nilsen F, Skogseth R, Vaardal-Lunde J, et al. 2016. A simple shelf circulation model: intrusion of Atlantic water on the West Spitsbergen shelf. J Phys Oceanogr, 46(4): 1209-1230, doi:10.1175/jpo-d-15- 0058.1.

Onarheim I H, Eldevik T, Smedsrud L H, et al. 2018. Seasonal and regional manifestation of Arctic Sea ice loss. J Climate, 31(12): 4917-4932, doi:10.1175/jcli-d-17-0427.1.

Overland J E, Wang M Y, Walsh J E, et al. 2014. Future Arctic climate changes: adaptation and mitigation time scales. Earth Future, 2(2): 68-74, doi:10.1002/2013EF000162.

Overland J, Dunlea E, Box J E, et al. 2019. The urgency of Arctic change. Polar Sci, 21: 6-13, doi:10.1016/j.polar.2018.11.008.

Polyakov I V, Bekryaev R V, Alekseev G V, et al. 2003. Variability and trends of air temperature and pressure in the maritime Arctic, 1875-2000. J Climate, 16(12): 2067-2077, doi:10.1175/1520-0442(2003)016<2067: vatoat>2.0.co;2.

Rigor I G, Colony R L, Martin S. 2000. Variations in surface air temperature observations in the Arctic, 1979-97. J Climate, 13(5): 896-914, doi:10.1175/1520-0442(2000)013<0896: visato>2.0.co;2.

Rudels B. 2010. Constraints on exchanges in the Arctic Mediterranean—do they exist and can they be of use? Tellus A Dyn Meteorol Oceanogr, 62(2): 109-122, doi:10.1111/j.1600-0870.2009.00425.x.

Svendsen H, Beszczynska-Møller A, Hagen J O, et al. 2002. The physical environment of Kongsfjorden-Krossfjorden, an Arctic fjord system in Svalbard. Polar Res, 21(1): 133-166, doi:10.3402/polar.v21i1.6479.

Trenberth K E, Stepaniak D P. 2003. Covariability of components of poleward atmospheric energy transports on seasonal and interannual timescales. J Climate, 16(22): 3691-3705, doi:10.1175/1520-0442(2003)016<3691: cocopa>2.0.co;2.

Walczowski W, Beszczynska-Möller A, Wieczorek P, et al. 2017. Oceanographic observations in the Nordic Sea and Fram Strait in 2016 under the IO PAN long-term monitoring program AREX. Oceanologia, 59(2): 187-194, doi:10.1016/j.oceano.2016.12.003.

Zhang J, Stegall S T, Zhang X D. 2018. Wind-sea surface temperature-sea ice relationship in the Chukchi-Beaufort Seas during autumn. Environ Res Lett, 13(3): 034008, doi:10.1088/1748-9326/aa9adb.

Zhang X D, He J X, Zhang J, et al. 2013. Enhanced poleward moisture transport and amplified northern high-latitude wetting trend. Nat Clim Change, 3(1): 47-51, doi:10.1038/nclimate1631.

Zillman J W. 2001. The IPCC third assessment report on the scientific basis of climate change. Australas J Environ Manag, 8(3): 169-185, doi:10.1080/14486563.2001.10648526.